arXiv:1810.09694v1 [nlin.AO] 23 Oct 2018

# The Key Player Problem in Complex Oscillator Networks and Electric Power Grids: Resistance Centralities Identify Local Vulnerabilities

M. Tyloo and L. Pagnier

*Institute of Physics, EPF Lausanne, CH-1015 Lausanne, Switzerland and*

*School of Engineering, University of Applied Sciences of*

*Western Switzerland HES-SO CH-1951 Sion, Switzerland*

Ph. Jacquod

*School of Engineering, University of Applied Sciences of*

*Western Switzerland HES-SO CH-1951 Sion, Switzerland*

(Dated: November 12, 2021)

## Abstract

Identifying key players in a set of coupled individual systems is a fundamental problem in network theory [1–3]. Its origin can be traced back to social sciences and the problem led to ranking algorithms based on graph theoretic centralities [4]. Coupled dynamical systems differ from social networks in that, first, they are characterized by degrees of freedom with a deterministic dynamics and second the coupling between individual systems is a well-defined function of those degrees of freedom. One therefore expects the resulting coupled dynamics, and not only the network topology, to also determine the key players. Here, we investigate synchronizable network-coupled dynamical systems such as high voltage electric power grids and coupled oscillators on complex networks. We search for network nodes which, once perturbed by a local noisy disturbance, generate the largest overall transient excursion away from synchrony. A spectral decomposition of the network coupling matrix leads to an elegant, concise, yet accurate solution to this identification problem. We show that, when the internodal coupling matrix is Laplacian, these key players are peripheral in the sense of a centrality measure defined from effective resistance distances. For linearly coupled dynamical systems such as weakly loaded electric power grids or consensus algorithms, the nodal ranking is efficiently obtained through a single Laplacian matrix inversion, regardless of the operational synchronous state. We call the resulting ranking index *LRank*. For heavily loaded electric power grids or coupled oscillators systems closer to the transition to synchrony, nonlinearities render the nodal ranking dependent on the operational synchronous state. In this case a weighted Laplacian matrix inversion gives another ranking index, which we call *WLRank*. Quite surprisingly, we find that LRank provides a faithful ranking even for well developed coupling nonlinearities, corresponding to oscillator angle differences up to $\Delta\theta \lesssim 40^o$ approximately.

## INTRODUCTION

Because of growing electric power demand, increasing difficulties with building new lines and the emergence of intermittent new renewable energy sources, electric power systems are more often operated closer to their maximal capacity [5, 6]. Accordingly, their operating state, its robustness against potential disturbances and its local vulnerabilities need to be assessed more frequently and precisely. Furthermore, because electricity markets become more and more integrated, it is necessary to perform these assessments over geographically larger areas. Grid reliability is commonly assessed against $n-1$ feasibility, transient stability and voltage stability, by which one means that a grid is considered reliable if (i) it still has an acceptable operating state after any one of its $n$ components fails, (ii) that acceptable state is reached from the original state following the transient dynamics generated by the component failure and (iii) the new operating state is robust against further changes in operating conditions such as changes in power productions and loads. This $n-1$ contingency assessment is much harder to implement in real-time for a power grid loaded close to its capacity where the differential equations governing its dynamics become nonlinear – the fast, standardly used linear approximation breaks down as the grid is more and more heavily loaded. Nonlinear assessment algorithms have significantly longer runtimes, which makes them of little use for short-time evaluations. In worst cases, they sometimes even do not converge. In short, heavily loaded grids need more frequent, more precise reliability assessments which are however harder to obtain, precisely because the loads are closer to the grid capacities.

Developing real-time procedures for $n-1$ contingency assessment requires new, innovative algorithms. One appealling avenue is to optimize contingency ranking [3] to try and identify a subset of $n_s < n$ grid components containing all the potentially critical components. The $n-1$ contingency assessment may then focus on that subset only, with a significant gain in runtime if $n_s \ll n$. Identifying such a subset requires a ranking algorithm for grid components, following some well-chosen criterion. Procedures of this kind have been developed in network models for social and computer sciences, biology and other fields, in the context of the historical and fundamental problem of identifying the *key players* [1, 2, 7, 8]. They may be for instance the players who, once removed, lead to the biggest changes in the other player's activity in game theory, or to the biggest structural change in a social network. That problem has been addressed with the introduction of graph theoretic centrality measures [4, 9] which order nodes from the most "central" to the most "peripheral" – in a sense that they themselves define. A plethora of centrality indices have been introduced and discussed in the literature on network theory [4, 9], culminating with PageRank [10].

The latter ranks nodes in a network according to the stationary probability distribution of a Markov chain on the network, accordingly it gives a meaningful ranking of websites under the reasonable assumption that websurfing is a random process. Their computational efficiency makes PageRank, as well as other purely graph theoretic indicators very attractive to identify key players on complex networks. It is thus quite tempting to apply purely graph theoretic methods to identify fast and reliably key players in network-coupled dynamical systems.

Processes such as web crawling for information retrieval are essentially random diffusive walks on a complex network, with no physical conservation law beyond the conservation of probability. The situation is similar for disease [11] or rumor [12] spreading, and for community formation [13] where graph theoretic concepts of index, centrality, betweenness, coreness and so forth have been successfully applied to identify tightly-bound communities. Coupled dynamical systems such as complex supply networks [14], electric power grids [15], consensus algorithm networks [16] or more generally network-coupled oscillators [17, 18] are however fundamentally different. There, the randomness of motion on the network giving e.g. the Markovian chain at the core of PageRank is replaced by a deterministic dynamics supplemented by physical conservation laws that cannot be neglected. Pure or partially extended graph theoretic methods have been applied in vulnerability investigations of electric power grids [19–21], and investigations of cascades of failures in coupled communication and electric power networks [22, 23]. They have however been partially or totally invalidated by investigations on more precise models of electric power transmission that take fundamental physical laws into account (in this case, Ohm's and Kirchhoff's laws) [24, 25]. It is therefore doubtful that purely topological graph theoretic descriptors are able to identify the potentially critical components in deterministic, network-coupled dynamical systems. Purely graph-theoretic approaches need to be extended to account for physical laws [19].

Here, we give an elegant solution to the key player problem for a family of deterministic, network-coupled dynamical systems related to the Kuramoto model [17, 18]. While we focus mostly on high voltage electric power grids whose swing dynamics, under the lossless line approximation, is given by a second-order version of the Kuramoto model [15, 26], we show that our approach also applies to other, generic models of network-coupled oscillators. Key players in such systems can be defined in various ways. For instance, they can be identified by an optimal geographical distribution of system parameters such as inertia, damping or natural frequencies or alternatively as those whose removal leads to the biggest change in operating state. In this article we define the key players as those nodes where a local disturbance leads to the largest network response. There are different measures to quantify the magnitude of the transient response, such as nadir and maximal rate of

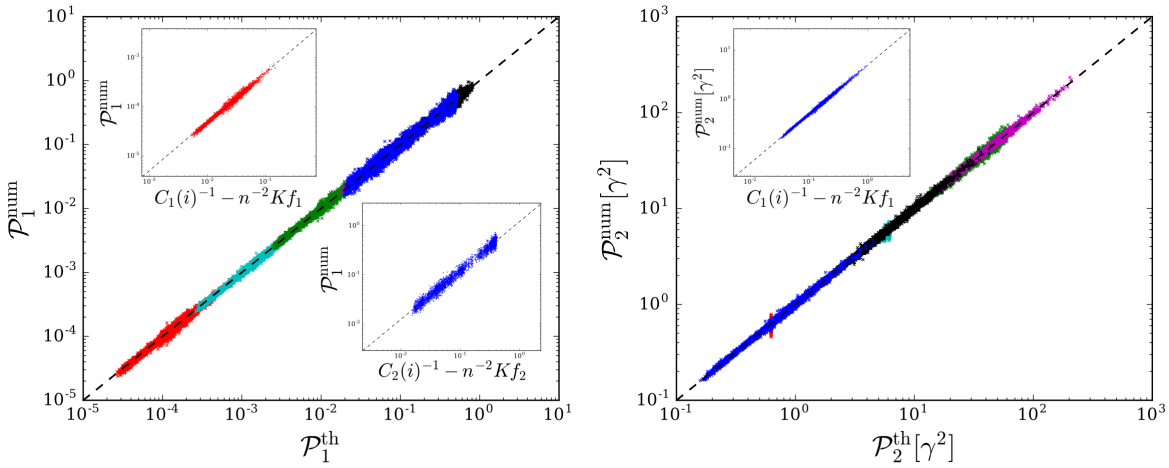



Figure 1. Comparison between theoretical predictions and numerical results for both performance measures $\mathcal{P}_1$ and $\mathcal{P}_2$ defined in Eqs. (3). Each point corresponds to a noisy disturbance on a single node of the European electric power grid sketched in Fig. 2a (supplementary materials, materials and methods) and governed by Eq. (1). The time-dependent disturbance $\delta P_i(t)$ is defined by an Ornstein-Uhlenbeck noise of magnitude $\delta P_0 = 1$ and correlation time $\gamma\tau_0 = 4\cdot10^{-5}$ (red crosses), $4\cdot10^{-4}$ (cyan), $4\cdot10^{-3}$ (green), $4\cdot10^{-2}$ (purple), $4\cdot10^{-1}$ (black) and 4 (blue). Time scales are defined by the ratio of damping to inertia coefficients $\gamma = d_i/m_i = 0.4s^{-1}$ which is assumed constant with $d_i = 0.02s$. The insets show $\mathcal{P}_1$ and $\mathcal{P}_2$ as a function of the resistance distance-based graph theoretic predictions of Eqs. (6) valid in both limits of very large and very short noise correlation time $\tau_0$. Not shown is the limit of short $\tau_0$ for $\mathcal{P}_2$, which gives a node-independent result, Eq. (6b).

change of the network-averaged frequency [27, 28] or other dynamical quantities such as network susceptibilities [29] and the wave dynamics following disturbances [30]. Here, we quantify the total transient excursion through performance measures that are time-integrated quadratic forms in the system's degrees of freedom (supplementary materials, materials and methods). Anticipating on results to come, Fig. 1 illustrates the excellent agreement between analytical theory and numerical calculations for such performance measures. Particularly interesting is that in both asymptotic limits of quickly and slowly decorrelating noisy disturbance, the performance measures are simply expressed in terms of the *resistance centrality* [31, 32], which is a variation of the closeness centrality [4] based on resistance distances [33]. This is shown in the insets of Fig. 1. Our main finding is that the resistance centrality is the relevant quantity to construct ranking algorithms in network-coupled dynamical systems.

## THE MODEL AND APPROACH

We consider network-coupled dynamical systems defined by sets of differential equations of the form

$$m_i\ddot{\theta}_i + d_i\dot{\theta}_i = P_i - \sum_j b_{ij}\sin(\theta_i - \theta_j)\,,\;\; i = 1, ..., n. \tag{1}$$

The coupled individual systems are oscillators with a compact, angle degree of freedom $\theta_i \in (-\pi, \pi]$. Their uncoupled dynamics are determined by natural frequencies $P_i$, inertia coefficients $m_i$ and damping coefficients $d_i$. Because the degrees of freedom are compact, the coupling between oscillators needs to be a periodic function of angle differences and here we keep only its first Fourier term. The coupling between pairs of oscillators is defined on a network whose Laplacian matrix has elements $\mathbb{L}^{(0)}_{ij} = -b_{ij}$ if $i \neq j$ and $\mathbb{L}^{(0)}_{ii} = \sum_{k\neq i} b_{ik}$. Without inertia, $m_i = 0\ \forall i$, Eq. (1) gives the celebrated Kuramoto model on a network with edge weights $b_{ij} > 0$, $\forall i, j$ [17, 18]. With inertia on certain nodes, it is an approximate model for the swing dynamics of high-voltage electric power grids in the lossless line limit [15, 26, 34]. When angle differences are small, a linear approximation $\sin(\theta_i - \theta_j) \simeq \theta_i - \theta_j$ is justified, giving first- (without) or second-order (with inertia) consensus dynamics [16].

When the natural frequencies $P_i$ are not too large, synchronous solutions exist that satisfy Eq. (1) with $\ddot{\theta}_i = 0$ and $\dot{\theta}_i = \omega_0$, $\forall i$. Without loss of generality, one may consider Eq. (1) in a frame rotating with the angular frequency $\omega_0$ in which case such synchronous states correspond to stable fixed points with $\dot{\theta}_i = 0$. We consider a fixed point with angle coordinates $\boldsymbol{\theta}^{(0)} = (\theta^{(0)}_1, \ldots, \theta^{(0)}_n)$ corresponding to natural frequencies $\boldsymbol{P}^{(0)} = (P^{(0)}_1, \ldots, P^{(0)}_n)$, to which we add a time-dependent disturbance, $P_i(t) = P^{(0)}_i + \delta P_i(t)$. Linearizing the dynamics about that solution, Eq. (1) becomes

$$m_i\delta\ddot{\theta}_i + d_i\delta\dot{\theta}_i = \delta P_i(t) - \sum_j b_{ij}\cos(\theta^{(0)}_i - \theta^{(0)}_j)(\delta\theta_i - \delta\theta_j)\,,\;\; i = 1, ..., n, \tag{2}$$

where $\delta\theta_i(t) = \theta_i(t) - \theta^{(0)}_i$. This set of coupled differential equations governs the small-signal response of the system corresponding to weak disturbances. The couplings are defined by a weighted Laplacian matrix $\mathbb{L}_{ij}(\boldsymbol{\theta}^{(0)}) = -b_{ij}\cos(\theta^{(0)}_i - \theta^{(0)}_j)$ if $i \neq j$ and $\mathbb{L}_{ii}(\boldsymbol{\theta}^{(0)}) = \sum_k b_{ik}\cos(\theta^{(0)}_i - \theta^{(0)}_k)$ which contains information on both the topology of the network and the operational state of the system. This weighted Laplacian matrix significantly differs from the network Laplacian $\mathbb{L}^{(0)}$ when angle differences between coupled nodes are large.

We assess the nodal vulnerability of the system defined in Eq. (1) via the magnitude of the transient dynamics determined by Eq. (2) under a time-dependent disturbance $\delta P_i(t)$. We take the

latter as an Ornstein-Uhlenbeck noise on the natural frequency of a single node, with vanishing average, $\overline{\delta P_i(t)} = 0$, variance $\delta P_0^2$ and correlation time $\tau_0$, $\overline{\delta P_i(t_1)\delta P_j(t_2)} = \delta_{ik}\,\delta_{jk}\,\delta P_0^2 \exp[-|t_1 - t_2|/\tau_0]$. It is sequentially applied on each of the $k = 1, \dots n$ nodes. This noisy test disturbance is designed to investigate network properties on different time scales by varying $\tau_0$ and identify the set of most vulnerable nodes as those where the system's response to $\delta P_k(t)$ is largest. We quantify the magnitude of the response to the disturbance with the following two performance measures [35]

$$\mathcal{P}_1 = \lim_{T\to\infty} T^{-1} \sum_i \int_0^T |\delta\theta_i(t) - \Delta(t)|^2 \mathrm{d}t \,, \tag{3a}$$

$$\mathcal{P}_2 = \lim_{T\to\infty} T^{-1} \sum_i \int_0^T |\delta\dot{\theta}_i(t) - \dot{\Delta}(t)|^2 \mathrm{d}t \,. \tag{3b}$$

They are similar to performance measures based on $\mathcal{L}_2$-norms previously considered in the context of electric power networks [27, 36–40] but differ from them in two respects. First, here we subtract the averages $\Delta(t) = n^{-1}\sum_j \delta\theta_j(t)$ and $\dot{\Delta}(t) = n^{-1}\sum_j \delta\dot{\theta}_j(t)$ because the synchronous state does not change under a constant angle shift. Without that subtraction, artificially large performance measures may be obtained, which reflect a constant angle drift of the synchronous operational state and not a large transient excursion. Second, we divide $\mathcal{P}_{1,2}$ by $T$ before taking $T \to \infty$ because we consider a noisy disturbance that is not limited in time and which would otherwise lead to diverging values of $\mathcal{P}_{1,2}$.

## PERFORMANCE MEASURES AND RESISTANCE CENTRALITIES

The performance measures $\mathcal{P}_{1,2}$ can be computed analytically from Eq. (2) via Laplace transforms (supplementary materials, materials and methods). For uniform damping and inertia, i.e. $d_i = d = \gamma m_i$, $\forall i$, in the two limits of long and short noise correlation time $\tau_0$, they can be expressed in terms of the resistance centrality of the node $k$ on which the noisy disturbance acts and of graph topological indices called generalized Kirchhoff indices [33, 35]. Both quantities are based on the resistance distance, which gives the effective resistance $\Omega_{ij}$ between any two nodes $i$ and $j$ on a fictitious electrical network where each edge is a resistor of magnitude given by the inverse edge weight in the network defined by the weighted Laplacian matrix. One obtains

$$\Omega_{ij}(\boldsymbol{\theta}^{(0)}) = \mathbb{L}^\dagger_{ii}(\boldsymbol{\theta}^{(0)}) + \mathbb{L}^\dagger_{jj}(\boldsymbol{\theta}^{(0)}) - \mathbb{L}^\dagger_{ij}(\boldsymbol{\theta}^{(0)}) - \mathbb{L}^\dagger_{ji}(\boldsymbol{\theta}^{(0)}) \,, \tag{4}$$

where $\mathbb{L}^\dagger$ denotes the Moore-Penrose pseudo-inverse of $\mathbb{L}$ [33]. The resistance centrality of the $k^{\text{th}}$ node is then defined as $C_1(k) = [n^{-1}\sum_j \Omega_{jk}]^{-1}$. It measures how central node $k$ is in the electrical

network, in terms of its average resistance distance to all other nodes. A network descriptor, the Kirchhoff index is further defined as [33]

$$Kf_1 \equiv \sum_{i<j} \Omega_{ij} \,. \tag{5}$$

Generalized Kirchhoff indices $Kf_p$ and resistance centralities $C_p(k)$ can be defined analogously from the $p^{\text{th}}$ power of the weighted Laplacian matrix, which is also a Laplacian matrix (supplementary materials, materials and methods). In terms of these quantities, the performance measures defined in Eqs. (3) depend on the value of the noise correlation time $\tau_0$ relative to the different time scales in the system. The latter are the ratios $d/\lambda_\alpha$ of the damping coefficient $d$ with the nonzero eigenvalues $\lambda_\alpha$, $\alpha = 2, \dots n$, of $\mathbb{L}(\boldsymbol{\theta}^{(0)})$ and the inverse ratio $\gamma^{-1} = m/d$ of damping to inertia coefficients. The performance measures take in particular the asymptotic values

$$\mathcal{P}_1 = \begin{cases} \left(\delta P_0^2 \tau_0/d\right)\left(C_1^{-1}(k) - n^{-2} Kf_1\right) & , \ \tau_0 \ll d/\lambda_\alpha, \gamma^{-1} \\ \delta P_0^2 \left(C_2^{-1}(k) - n^{-2} Kf_2\right) & , \ \tau_0 \gg d/\lambda_\alpha, \gamma^{-1} \end{cases} \tag{6a}$$

$$\mathcal{P}_2 = \begin{cases} \left(\delta P_0^2 \tau_0/dm\right)\big(n-1\big)/n & , \ \tau_0 \ll d/\lambda_\alpha, \gamma^{-1} \\ \left(\delta P_0^2/d\tau_0\right)\left(C_1^{-1}(k) - n^{-2} Kf_1\right) & , \ \tau_0 \gg d/\lambda_\alpha, \gamma^{-1}, \end{cases} \tag{6b}$$

in the two limits when $\tau_0$ is the smallest or the largest time scale in the system. After averaging over the location $k$ of the disturbed node, $\overline{C_{1,2}} = 2Kf_{1,2}/n^2$, and one recovers the results of Refs. [35, 37, 38] for the global robustness of the system.

These results are remarkable : they show that the magnitude of the transient excursion under a local noisy disturbance is given by either of the generalized resistance centralities $C_1(k)$ or $C_2(k)$ of the perturbed node and the generalized Kirchhoff indices $Kf_{1,2}$. The latter are global network descriptors and are therefore fixed in a given network with fixed operational state. One concludes that perturbing the less central nodes – those with largest inverse centralities $C_{1,2}^{-1}(k)$ – generates the largest transient excursion. The asymptotic analytical results of Eqs. (6) are corroborated by numerical results in the insets of Fig.1, obtained directly from Eq. (1), i.e. without the linearization of Eq. (2). The validity of the general analytical expressions valid for any $\tau_0$ (supplementary materials, materials and methods) is further confirmed in the main panel of Fig. 1, and by further numerical results obtained for different networks shown in the supplementary materials, materials and methods.

The generalized resistance centralities and Kirchhoff indices appearing in Eqs. (6) depend on the operational state via the weighted Laplacian $\mathbb{L}(\boldsymbol{\theta}^{(0)})$. For a narrow distribution of natural frequencies $P_i \ll \sum_j b_{ij}$, $\forall i$, angle differences between coupled nodes remain small, and the weighted

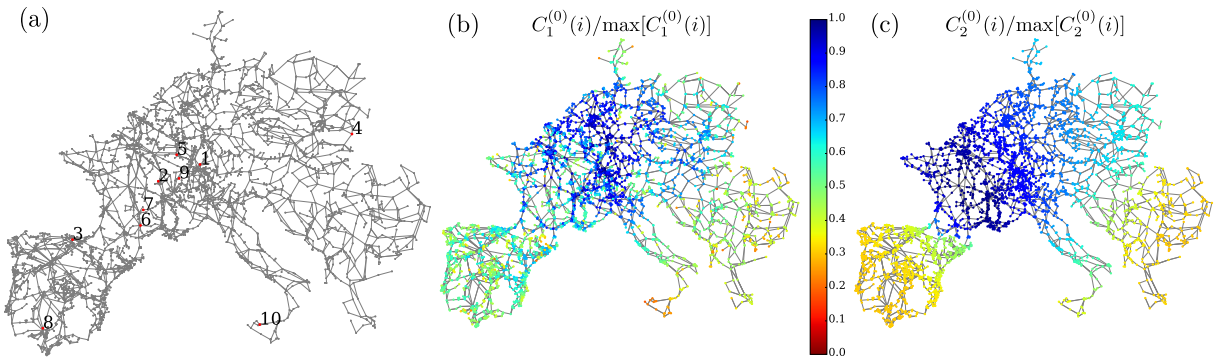



Figure 2. (a) Topology of the European electric power grid (supplementary materials, materials and methods) and location of the ten test nodes listed in Table I. Normalized generalized resistance centralities $C_1^{(0)}(i)$ (b), and $C_2^{(0)}(i)$ (c) for the network Laplacian matrix of the European electric power grid.

Laplacian is close to the network Laplacian, $\mathbb{L}(\boldsymbol{\theta}^{(0)}) \simeq \mathbb{L}^{(0)}$. The resistance centralities $C_1^{(0)}$ and $C_2^{(0)}$ for the network Laplacian of the European electric power grid are shown in Fig. 2. For both centralities, the less central nodes are dominantly located in the Balkans and Spain. Additionally, for $C_1^{(0)}$, nodes in Denmark and Sicily are also among the most peripheral. The general pattern of these most peripheral nodes looks very similar to the pattern of most sensitive nodes numerically found in Ref. [41], and includes in particular many, but not all dead ends, which have been numerically found to undermine grid stability [42].

The asymptotic results of Eqs. (6), together with the numerical results of Fig. 1 make a strong point that nodal sensitivity to fast or slowly decorrelating noise disturbances can be predicted by generalized resistance centralities. One may wonder at this point how generalized resistance centralities differ in that prediction from other, more common centralities such as geodesic centrality, nodal degree or PageRank. Table I compares these centralities to each other and to the performance measures corresponding to slowly decorrelating noisy disturbances acting on the ten nodes shown in Fig. 2a. As expected from Eq. (6), $\mathcal{P}_1$ and $\mathcal{P}_2$ are almost perfectly correlated with the inverse resistance centralities $C_2^{-1}$ and $C_1^{-1}$ respectively, but with no other centrality metrics. For the full set of nodes of the Europen electric power grid, we found Pearson correlation coefficients $\rho(\mathcal{P}_1, C_2^{-1}) = 0.997$, and $\rho(\mathcal{P}_2, C_1^{-1}) = 0.975$ fully corroborating the prediction of Eq. (6).

## RANKING OF LOCAL VULNERABILITIES

Once a one-to-one relation between the generalized resistance centralities $C_1(k)$ and $C_2(k)$ of the disturbed node $k$ and the magnitude of the induced transient response is established, ranking of

| node # | $C_{\text{geo}}$ | Degree | PageRank | $C_1$ | $C_2$ | $\mathcal{P}_1^{\text{num}}$ | $\mathcal{P}_2^{\text{num}}$ $[\gamma^2]$ |
|---|---|---|---|---|---|---|---|
| 1 | 7.84 | 4 | 3024 | 31.86 | 5.18 | 0.047 | 0.035 |
| 2 | 6.8 | 1 | 2716 | 22.45 | 5.68 | 0.021 | 0.118 |
| 3 | 5.56 | 10 | 896 | 22.45 | 2.33 | 0.32 | 0.116 |
| 4 | 4.79 | 3 | 1597 | 21.74 | 3.79 | 0.126 | 0.127 |
| 5 | 7.08 | 1 | 1462 | 21.74 | 5.34 | 0.026 | 0.125 |
| 6 | 4.38 | 6 | 2945 | 21.69 | 5.65 | 0.023 | 0.129 |
| 7 | 5.11 | 2 | 16 | 19.4 | 5.89 | 0.016 | 0.164 |
| 8 | 4.15 | 6 | 756 | 19.38 | 1.83 | 0.453 | 0.172 |
| 9 | 5.06 | 1 | 1715 | 10.2 | 5.2 | 0.047 | 0.449 |
| 10 | 2.72 | 4 | 167 | 7.49 | 2.17 | 0.335 | 0.64 |

Table I. Centrality metrics and performance measures $\mathcal{P}_{1,2}$ for the European electric power grid (supplementary materials, materials and methods) with noisy disturbances with large correlation time $\tau_0$ applied on the nodes shown in Fig. 2a. The performance measures $\mathcal{P}_1$ and $\mathcal{P}_2$ are almost perfectly correlated with the resistance centralities $C_2$ and $C_1$, but neither with the geodesic centrality, nor the degree, nor PageRank.

nodes from most to least critical is tantamount to ranking them from smallest to largest $C_1$ or $C_2$. From Eqs. (6), which of these two centralities is relevant depends on whether one is interested (i) in the transient response under fast or slowly decorrelating noise, or (ii) in investigating transient behaviors for angles (using the performance measure $\mathcal{P}_1$) or frequencies ($\mathcal{P}_2$). Quite interestingly, while this gives a priori four different rankings, Eqs. (6) lead to only two rankings, either based on $C_1^{-1}$ or $C_2^{-1}$, which can be obtained through the performance measure $\mathcal{P}_1$ only, in either asymptotic limit of very fast (shortest time scale $\tau_0$) or very slowly (largest $\tau_0$) decorrelating noise. From here on, we therefore focus on the angle performance measure $\mathcal{P}_1$ of Eq. (3a) and consider the two asymptotic limits in Eq. (6a).

We therefore define $\text{WLRank}_1$ and $\text{WLRank}_2$ [43] as two rankings which order nodes from smallest to largest $C_1$ and $C_2$ respectively. Fig. 3 shows that they differ very significantly. In particular a number of nodes are among the most critical according to $\text{WLRank}_1$ but not to $\text{WLRank}_2$ and vice-versa. This discrepancy means that nodes are not central in an absolute sense, instead, their centrality and hence how critical they are depends on details of the disturbance – in the present case, the correlation time $\tau_0$ – and the perfomance measure of interest. One should therefore chose to use one or the other centrality measure, according to the network sensitivity one wants to check.

The resistance centralities in Eqs. (6) correspond to the network defined by the weighted Lapla-

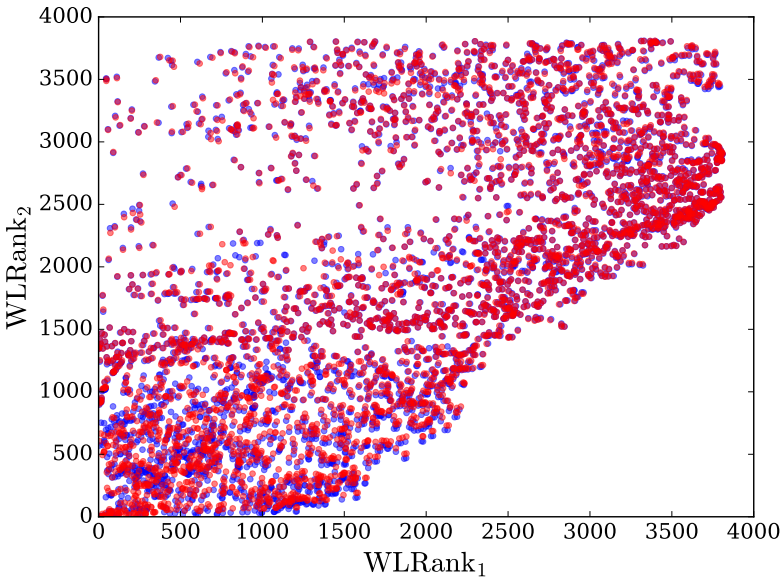



Figure 3. Comparison of the two nodal rankings $\mathrm{WLRank}_1$ and $\mathrm{WLRank}_2$ obtained from the generalized resistance centralities $C_1$ and $C_2$ respectively for the 3809 nodes of the European electric power grid sketched in Fig. 2a (supplementary materials, materials and methods). Blue dots correspond to a moderate load during a standard winter weekday and red dots to a significantly heavier load corresponding to the exceptional November 2016 situation with a rather large consumption and twenty french nuclear reactors shut down.

cian $\mathbb{L}(\boldsymbol{\theta}^{(0)})$ defined by Eq. (2). They therefore depend on the unperturbed, operating state $\boldsymbol{\theta}^{(0)}$, consequently, WLRank depends not only on the nework topology, but also, as expected, on the natural frequencies and the coupling between the nodal degrees of freedom. As mentioned above, in the strong coupling limit, angle differences between coupled nodes remain small and $\mathbb{L}(\boldsymbol{\theta}^{(0)}) \simeq \mathbb{L}^{(0)}$. In that limit, one therefore expects nodal ranking to be given by resistance distances corresponding to the network Laplacian $\mathbb{L}^{(0)}$. How long this remains true is of central interest and to answer this question we define further rankings $\mathrm{LRank}_{1,2}$ as the rankings using resistance centralities $C^{(0)}_{1,2}$ obtained from the network Laplacian $\mathbb{L}^{(0)}$. As long as angle differences between network-coupled nodes are not too large, the ranking LRank based on the network Laplacian matrix is almost the same as the ranking true WLRank based on the weighted Laplacian. This is shown in Fig. 4 for three electric power grid models and one random network of coupled oscillators. For the electric power grid models, injections/natural frequencies are limited by the standard operational constraint that the thermal limit of each power line is at most only weakly exceeded. This corresponds approximately to a maximal angle difference of $\max(\Delta\theta) \simeq 30^o$ between any pair of coupled nodes. Accordingly, we find that even in relatively strongly loaded power grids (corresponding for instance to the exceptional situation of the fall of 2016 when twenty french nuclear reactors were

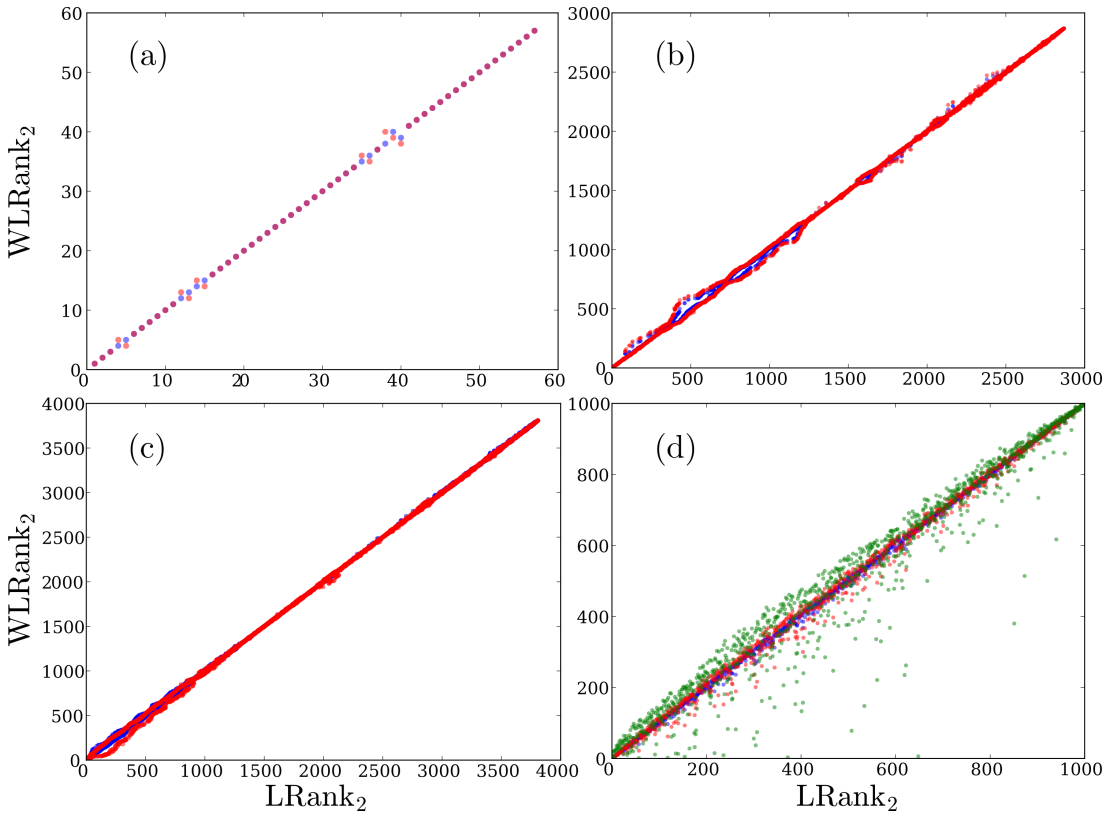



Figure 4. Comparison between LRank and WLRank corresponding to $\mathcal{P}_1$ for noisy disturbances with large correlation time $\tau_0$. (a–c) Electric power grid models for normally (blue) and more heavily loaded (red) operating states governed by Eq. (1). (a) IEEE 57 testcase where the more loaded case has injections six times larger than the moderately loaded, tabulated case [44]. (b) Pegase 2869 testcase where the more loaded case has injections 30% larger than the moderately loaded, tabulated case [45]. (c) European electric power grid model sketched in Fig. 2a (supplementary materials, materials and methods) where the moderately loaded case corresponds to a standard winter weekday and the more heavily loaded case to the November 2016 situation with twenty french nuclear reactors offline. (d) Inertialess coupled oscillators governed by Eq. (1) with $m_i = 0$, $\forall i$, on a random network with 1000 nodes obtained by rewiring a cyclic graph with constant nearest and next-to-nearest neighbor coupling with probability 0.5 (supplementary materials, materials and methods) [46]. Natural frequencies are randomly distributed as $P_i \in [-1.8, 1.63]$ (blue), $P_i \in [-2.16, 1.95]$ (red) and $P_i \in [-2.7, 2.45]$ (green), corresponding to maximal angle differences $\max(\Delta\theta) = 31^o$, $70^o$ and $106^o$ respectively.

simultaneously offline; see red points in Fig. 4c, there is not much of a difference between LRank and WLRank. The two rankings start to differ from one another only when at least some natural frequencies become comparable with the corresponding nodal index, $P_i \lesssim \sum_j b_{ij}$, and angle differences become very large. This case has been investigated for an inertialess coupled oscillator system on a random rewired network with constant couplings (supplementary materials, materials and methods) [46]. It is shown in green in Fig. 4d and corresponds to $\max(\Delta\theta) = 106^o$.

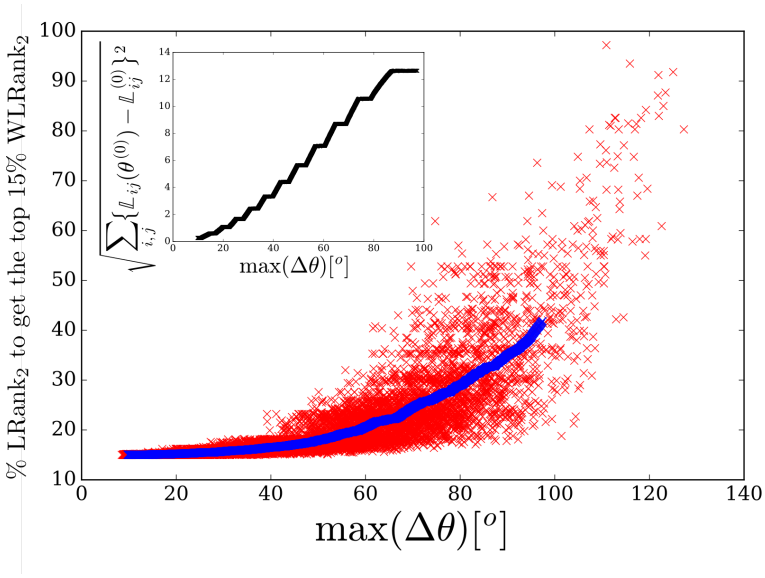



Figure 5. Percentage of the nodes with highest LRank$_2$ necessary to give the top 15 % ranked nodes with WLRank$_2$ for a random network of inertialess coupled oscillators with 1000 nodes obtained by rewiring with probability 0.5 a cyclic network with constant nearest and next-to-nearest neighbor coupling (supplementary materials, materials and methods) [46]. Each of the 12000 red crosses corresponds to one of 1000 random natural frequency vector $\boldsymbol{P}^{(0)}$ with components randomly distributed in $[-0.5, 0.5]$ and summing to zero, multiplied by a prefactor $\beta = 0.4, 0.6, \ldots 2.4, 2.6$. The blue crosses correspond to running averages over 500 red crosses with consecutive values of $\max(\Delta\theta)$. Inset : running averages of the Frobenius distance between the matrices $\mathbb{L}(\boldsymbol{\theta}^{(0)})$ and $\mathbb{L}^{(0)}$. The steps in the curve reflect discrete increments of $\beta$.

In Fig. 5 we investigate more closely when the approximate ranking LRank starts to differ from the true ranking WLRank. To that end we used the randomly rewired model of inertialess coupled oscillators of Fig. 4d and calculated the percentage of nodes with highest LRank$_2$ necessary to give the top 15 % ranked nodes with WLRank$_2$. The results are plotted as a function of the maximal angle difference between directly coupled nodes. Each of the 12000 red crosses in Fig. 5 corresponds to one of 1000 natural frequency vectors $\boldsymbol{P}^{(0)}$, with components randomly distributed in $[-0.5, 0.5]$ and summing to zero, multiplied by a prefactor $\beta = 0.4, 0.6, \ldots 2.4, 2.6$. The blue crosses correspond to running averages over 500 red crosses with consecutive values of $\max(\Delta\theta)$. One sees that, up to almost $\max(\Delta\theta) \simeq 40^o$, the set of the 18 % of nodes with highest LRank$_2$ always includes the top 15 % ranked nodes with WLRank$_2$. Similar results for obtaining the top 10 and 20 % ranked nodes with WLRank$_2$, and for rankings using $C_1$ instead of $C_2$ are shown in the supplementary materials, materials and methods.

That nodal ranking remains almost the same up to angle differences of about $40^o$ is quite sur-

prising, since coupling nonlinearities are already well developed there. This is illustrated in the inset of Fig. 5 which plots the Frobenius distance $\sqrt{\sum_{ij}\left(\mathbb{L}_{ij}(\boldsymbol{\theta}^{(0)})-\mathbb{L}_{ij}^{(0)}\right)^2}$ between the network Laplacian $\mathbb{L}^{(0)}$ and the weighted Laplacian $\mathbb{L}(\boldsymbol{\theta}^{(0)})$. When $\max(\Delta\theta)\simeq 40^o$, the Frobenius distance has already reached about 27 % of its maximal observed value, indicating that coupling nonlinearities are already significant. Yet, obtaining a desired set of the $n_s$ most critical nodes for any configuration with $\max(\Delta\theta)\lesssim 40^o$, including cases with nonegligible nonlinearities, is achieved with a single matrix inversion of the network Laplacian $\mathbb{L}^{(0)}$, while considering a slightly extended set of $n_s+\delta n_s$ nodes with highest LRank, $\delta n_s/n_s \ll 1$. This is a moderate price to pay, compared to the price of calculating WLRank for each configuration, which each time requires inverting the weighted Laplacian matrix $\mathbb{L}(\boldsymbol{\theta}^{(0)})$. That latter procedure would be too-time consuming for real-time assessment of large networks.

## CONCLUSION

We have formulated a key player problem in deterministic, network-coupled dynamical systems. The formulation is based on the dynamical response to a nodal additive disturbance of the initial problem, and the most critical nodes – the key players – are defined as those where the response to the disturbance is largest. While this manuscript focused on (i) noisy Ornstein-Uhlenbeck disturbances, (ii) network-coupled systems on undirected graphs, in particular with symmetric couplings $b_{ij}=b_{ji}$ in Eq. (1), and (iii) performance measures of the transient response that are quadratic forms in the system's degrees of freedom, the method is not restricted to such cases. First, it can be used to deal with different disturbances and in the supplementary materials, materials and methods, we calculate $\mathcal{P}_{1,2}$ for a box disturbance $\delta P_i(t)=\delta_{ik}\delta P_0\Theta(t)\Theta(\tau_0-t)$ with the Heaviside function $\Theta(t)$. Remarkably, this disturbance gives the same ranking as the Ornstein-Uhlenbeck noise disturbance considered above. Second, asymmetric couplings occurring e.g. in directed graphs [47], in Kuramoto models with frustration [18] or in electric power grids with Ohmic dissipation [15] can also be considered. In this case, the internodal coupling is given by asymmetric real matrices instead of symmetric Laplacian matrices. However, the definition of the resistance distance, Eq. (4), remains valid even if $\mathbb{L}$ is replaced by an asymmetric matrix $\mathbb{A}$, in that it still gives $\Omega_{ii}=0$, $\Omega_{ij}\geq 0$, and $\Omega_{ij}\leq\Omega_{ik}+\Omega_{ki}$, $\forall i,j,k$ as long as the synchronous fixed point considered remains stable. Third, nonquadratic performance measures can in principle be considered within the spectral decomposition used in this article. One may think of average frequency nadir and rate of change of frequency, which are linear performance measures [27, 28].

It is at present unclear whether these quantities can be analytically related to the location of disturbances via resistance or other centralities.

We gave an elegant answer to this key player problem : ranking nodes from most to least critical is tantamount to ranking nodes from least to most central in the sense of resistance centralities. Depending on how the problem is formulated – mostly on details of the disturbance as well as on how the magnitude of the transient response is measured – different centralities have to be considered, giving different rankings. The key player problem in deterministic systems is therefore not uniquely defined and its formulation must be tailored to reflect the most relevant dynamical properties one wants to evaluate. Averaged rankings, reflecting several such properties simultaneously could also be considered.

## ACKNOWLEDGMENTS

This work has been supported by the Swiss National Science Foundation under an AP Energy Grant. We thank Robin Delabays and Tommaso Coletta for interesting discussions.

[1] C. Ballester, A. Calvó-Armengol, and Y. Zenou, *Who's Who in Networks. Wanted : the Key Player*, Econometrica **74**, 1403 (2006).

[2] S.P. Borgatti, *Identifying Sets of Key Players in a Social Network*, Comput. Math. Organiz. Theor. **12**, 21 (2006); *Centrality and Network Flow*, Soc. Netw. **27**, 55 (2005).

[3] S. Fliscounakis, P. Panciatici, F. Capitanescu, and L. Wehenkel, *Contingency Ranking With Respect to Overloads in Very Large Power Systems Taking Into Account Uncertainty, Preventive, and Corrective Actions*, IEEE Transactions on Power Systems **28**, 4909 (2013).

[4] P. Boldi and S. Vigna, *Axioms for Centrality*, Internet Mathematics **10**, 222 (2014).

[5] D. Kramer, *Models Poised to Boost Grid Efficiency*, Phys. Today **9**, 25 (2016).

[6] *Analytic Research Foundations for the Next-Generation Electric Grid*, Report from the National Academies of Sciences, Engineering and Medicine, available online at www.nap.edu/catalog/21919.

[7] R.V. Solé and J.M. Montoya, *Complexity and fragility in ecological networks*, Proc. R. Soc. Lond. B **268**, 2039 (2001).

[8] J.M. Montoya, S.L. Pimm, and R.V. Solé, *Ecological networks and their fragility*, Nature **442**, 259 (2006).

[9] P. Bonacich, *Power and Centrality : A Family of Measures*, Amer. J. Sociol. **92**, 1170 (1987).

[10] S. Brin and L. Page, *The Anatomy of a Large-Scale Hypertextual Web Search Engine*, Comput. Netw. ISDN Syst. **30** 107 (1998).

[11] M. Kitsak, L.K. Gallos, S. Havlin, F. Liljeros, L. Muchnik, H.E. Stanley, and H.A. Makse, *Identification of influential spreaders in complex networks*, Nature Physics **6**, 888 (2010).

[12] J. Borge-Holthoefer and Y. Moreno, *Absence of Influential Spreaders in Rumor Dynamics*, Phys. Rev. E **85**, 026116 (2012).

[13] M. Girvan and M.E.J. Newman, *Community Structure in Social and Biological Networks*, Proc. Natl. Acad. Sci. USA **99**, 7821 (2002).

[14] M. Herty, *Gas Flow in Pipeline Networks*, Networks and Heterogeneous Media **1**, 41 (2006).

[15] J. Machowski, J.W. Bialek, and J.R. Bumby, *Power System Dynamics: Stability and Control* 2nd Ed., John Wiley and Sons (2011).

[16] N.A. Lynch, *Distributed Algorithms*, Morgan Kaufmann Publishers (1997).

[17] Y. Kuramoto, in *International Symposium on Mathematical Problems in Theoretical Physics*, Lecture Notes in Physics **39**, 420 (Springer, New York, 1975).

[18] J.A. Acebrón, L.L. Bonilla, C.J. Pérez Vicente, F. Ritort, and R. Spigler, *The Kuramoto Model: A Simple Paradigm for Synchronization Phenomena*, Rev. Mod. Phys. **77**, 137 (2005).

[19] E. Bompard, E. Pons, and D. Wu, *Analysis of the Structural Vulnerability of the Interconnected Power Grid of Continental Europe with the Integrated Power System and Unified Power System Based on Extended Topological Approach*, Int. Transactions Electr. Energy Syst. **23**, 620 (2013).

[20] J.L. Sanchez Torres, *Vulnérabilité, Interdépendance et Analyse des Risques des Postes Sources et des Modes d'Exploitation Décentralisés des Réseaux Electriques*, PhD Thesis, University of Grenoble (2013).

[21] K.N. Hasan, R. Preece, and J.V. Milanović, *Priority Ranking of Critical Uncertainties Affecting Small-Disturbance Stability Using Sensitivity Analysis Techniques*, IEEE Transactions on Power Systems **32**, 2629 (2017).

[22] S.V. Buldyrev, R. Parshani, G. Paul, H.E. Stanley, and S. Havlin, *Catastrophic Cascade of Failures in Interdependent Networks*, Nature **464**, 1025 (2010).

[23] A. Basgan, Y. Berezin, S.V. Buldyrev, and S. Havlin, *The Extreme Vulnerability of Interdependent Spatially Embedded Networks*, Nat. Phys. **9** 667 (2013).

[24] P. Hines, E. Cotilla-Sanchez, and S. Blumsack, *Do Topological Models Provide Good Information about Electricity Infrastructure Vulnerability?*, Chaos **20**, 033122 (2010).

[25] M. Korkali, J.G. Veneman, B.F. Tivnan, and P.D.H. Hines, *Reducing Cascading Failure Risk by Increasing Infrastructure Network Interdependency*, Sci. Rep. **7**, 44499 (2017).

[26] F. Dörfler, M. Chertkov, and F. Bullo, *Synchronization in Complex Oscillator Networks and Smart Grids*, Proc. Natl Acad. Sci. **110**, 2005 (2013).

[27] F. Paganini and E. Mallada, *Global Performance Metrics for Synchronization of Heterogeneously Rated Power Systems: The Role of Machine Models and Inertia*, Proceedings of the 55$^{\text{th}}$ Allerton Conference on Communication, Control, and Computing, 324 (2017).

[28] L. Guo, G. Zhao, and S.H. Low, *Graph Laplacian Spectrum and Primary Frequency Regulation*, arXiv.org:1803.03905 (2018).

[29] D. Manik, M. Rohden, H. Ronellenfitsch, X. Zhang, S. Hallerberg, D. Witthaut, and M. Timme, *Network Susceptibilities : Theory and Applications*, Phys. Rev. E **95**, 012319 (2017).

[30] S. Tamrakar, M. Conrath, and S. Kettemann, *Propagation of Disturbances in AC Electricity Grids*, Sci. Rep. **8**, 6459 (2018).

[31] K.A. Stephenson and M. Zelen, *Rethinking centrality: Methods and examples*, Social Networks **11**, 1 (1989).

[32] U. Brandes and D. Fleischer, *Centrality Measures Based on Current Flow*, Proc. 22$^{\text{nd}}$ Symposium on Theoretical Aspects of Computer Science, 533 (2005).

[33] D.J. Klein and M. Randić, *Resistance Distance*, J. Math. Chem. **12**, 81 (1993).

[34] A.R. Bergen and D.J. Hill, *A Structure Preserving Model for Power System Stability Analysis*, IEEE Trans. Power App. Syst. **PAS-100**, 25 (1981).

[35] M. Tyloo, T. Coletta, and Ph. Jacquod, *Robustness of Synchrony in Complex Networks and Generalized Kirchhoff Indices*, Phys. Rev. Lett. **120**, 084101 (2018).

[36] E. Tegling, B. Bamieh and D.F. Gayme, *The Price of Synchrony: Evaluating the Resistive Losses in Synchronizing Power Networks*, IEEE Transactions on Control of Network Systems **2**, 254 (2015).

[37] M. Siami and N. Motee, *Systemic Measures for Performance and Robustness of Large-Scale Interconnected Dynamical Networks*, Proceedings of the 53$^{\text{rd}}$ IEEE Conference on Decision and Control, 5119 (2014).

[38] M. Siami and N. Motee, *Fundamental Limits and Tradeoffs on Disturbance Propagation in Linear Dynamical Networks*, IEEE Transactions on Automatic Control **61**, 4055 (2016).

[39] B.K. Poolla, S. Bolognani and F. Dörfler, *Optimal Placement of Virtual Inertia in Power Grids*, IEEE Transactions on Automatic Control **62**, 6209 (2017).

[40] T. Coletta and Ph. Jacquod, *Performance Measures in Electric Power Networks under Line Contingencies*, arXiv:1711.10348v2 (2018).

[41] L.V. Gambuzza, A. Buscarino, L. Fortuna, M. Porfiri, and M. Frasca, *Analysis of Dynamical Robustness to Noise in Power Grids*, IEEE Journal on Emerging and Selected topics in Circuits and Systems **7**, 413 (2017).

[42] P.J. Menck, J. Heitzig, J. Kurths, and H.J. Schellnhuber, *How Dead Ends Undermine Power Grid Stability*, Nature Communications **5**, 3969 (2014).

[43] When used, subscripts $\text{LRank}_i$ and $\text{WLRank}_i$ indicate that these are rankings obtained from the centralities $C_i$, $i = 1, 2$.

[44] University of Washington, Electrical Engineering, *Power Systems Test Case Archive*, available online at www2.ee.washington.edu/research/pstca (1993).

[45] R. D. Zimmerman, C. E. Murillo-Sánchez, and R. J. Thomas, *MATPOWER: Steady-State Operations, Planning and Analysis Tools for Power Systems Research and Education*, IEEE Trans. on Power Systems **26**, 12 (2011).

[46] D.J. Watts and S.H. Strogatz, *Collective Dynamics of 'Small World' Networks*, Nature **393**, 440 (1998).

[47] R. Delabays, Ph. Jacquod and F. Dörfler, *The Kuramoto Model on Directed and Signed Graphs*, arXiv:1807.11410 (2018).

# Supplementary Material for
# The Key Player Problem in Complex Oscillator Networks and Electric Power Grids: Resistance Centralities Identify Local Vulnerabilities

## CALCULATION OF THE PERFORMANCE MEASURES

We give some details of the calculation of the performance measures, Eqs. (3) in the main text. These calculations generalize to second-order swing equations the results obtained for the first-order Kuramoto model in Ref. [S1]. Starting from Eq. (1) in the main text, we consider a stable fixed-point solution $\boldsymbol{\theta}^{(0)} = (\theta_1^{(0)}, \ldots, \theta_n^{(0)})$ with unperturbed natural frequencies $\boldsymbol{P}^{(0)}$. We subject this state to a time-dependent disturbance $\boldsymbol{P}(t) = \boldsymbol{P}^{(0)} + \delta\boldsymbol{P}(t)$, which makes angles become time-dependent, $\boldsymbol{\theta}(t) = \boldsymbol{\theta}^{(0)} + \delta\boldsymbol{\theta}(t)$. Linearizing the dynamics defined by Eq. (1) of the main text about $\boldsymbol{\theta}^{(0)}$ and under the assumption that $d_i/m_i = \gamma$, $\forall i$, one obtains

$$\delta\ddot{\bar{\boldsymbol{\theta}}} + \gamma\delta\dot{\bar{\boldsymbol{\theta}}} = \boldsymbol{M}^{-1/2}\delta\boldsymbol{P} - \boldsymbol{M}^{-1/2}\mathbb{L}(\boldsymbol{\theta}^{(0)})\boldsymbol{M}^{-1/2}\,\delta\bar{\boldsymbol{\theta}}\,, \tag{S1}$$

where we introduced matrices with elements $D_{ij} = \delta_{ij}\,d_i = \gamma M_{ij}$ and new angle coordinates $\delta\bar{\boldsymbol{\theta}} = \boldsymbol{M}^{1/2}\delta\boldsymbol{\theta}$. The weighted Laplacian matrix $\mathbb{L}(\boldsymbol{\theta}^{(0)})$ is defined as

$$\mathbb{L}_{ij} = \begin{cases} -b_{ij}\cos(\theta_i^{(0)} - \theta_j^{(0)})\,, & i \neq j\,, \\ \sum_k b_{ik}\cos(\theta_i^{(0)} - \theta_k^{(0)})\,, & i = j\,. \end{cases} \tag{S2}$$

This Laplacian is minus the stability matrix of the linearized dynamics about a stable synchronous state. It is therefore positive semidefinite, with its largest eigenvalue $\lambda_1 = 0$ corresponding to a constant eigenvector $\mathbf{u}_1 = (1,1,1,...1)/\sqrt{n}$, and $\lambda_\alpha > 0$, $\alpha = 2,3,...n$. We define the matrix $\mathbb{L}^M = \boldsymbol{M}^{-1/2}\mathbb{L}\boldsymbol{M}^{-1/2}$ with eigenvectors $\mathbf{u}_\alpha^M$ and eigenvalues $\lambda_\alpha^M$, for $\alpha = 1,2,...n$. To calculate the response of the system to $\delta\boldsymbol{P}(t)$, we expand angle deviations over the eigenstates $\mathbf{u}_\alpha^M$ of $\mathbb{L}^M$, $\delta\bar{\boldsymbol{\theta}}(t) = \sum_\alpha c_\alpha(t)\,\mathbf{u}_\alpha^M$. Eq. (S1) becomes

$$\ddot{c}_\alpha(t) + \gamma\dot{c}_\alpha(t) = \boldsymbol{M}^{-1/2}\delta\boldsymbol{P}(t)\cdot\mathbf{u}_\alpha^M - \lambda_\alpha^M c_\alpha(t)\,. \tag{S3}$$

The disturbance starts at $t = 0$ and therefore $\delta\bar{\boldsymbol{\theta}}(0) = 0$ and $\delta\dot{\bar{\boldsymbol{\theta}}}(0) = 0$. Performing a Laplace transform on Eq. (S3), one gets

$$s^2 c_\alpha(s) + \gamma\, s\, c_\alpha(s) = \lambda_\alpha^M c_\alpha(s) + (\boldsymbol{M}^{-1/2}\delta\boldsymbol{P}\cdot\mathbf{u}_\alpha^M)(s)\,, \tag{S4}$$

where $c_\alpha(s) = \int_0^t e^{-st'}c_\alpha(t')dt'$ and $(\boldsymbol{M}^{-1/2}\delta\boldsymbol{P}\cdot\mathbf{u}_\alpha^M)(s) = \int_0^t e^{-st'}\boldsymbol{M}^{-1/2}\delta\boldsymbol{P}(t')\cdot\mathbf{u}_\alpha^M\,dt'$. Finally one obtains the Laplace transformed expansion coefficients of the angles over the eigenbasis of $\mathbf{u}_\alpha^M$

of $\mathbb{L}^M$,

$$c_\alpha(s) = (\boldsymbol{M}^{-1/2}\delta\boldsymbol{P}\cdot\mathbf{u}_\alpha^M)(s)\Big/\left(s-\frac{-\gamma+\Gamma_\alpha}{2}\right)\left(s+\frac{\gamma+\Gamma_\alpha}{2}\right)\,, \tag{S5}$$

with $\Gamma_\alpha = \sqrt{\gamma^2-4\lambda_\alpha^M}$. Applying an inverse Laplace transform leads to,

$$c_\alpha(t) = e^{\frac{-\gamma-\Gamma_\alpha}{2}t}\int_0^t e^{\Gamma_\alpha t'}\int_0^{t'}\boldsymbol{M}^{-1/2}\delta\boldsymbol{P}(t'')\cdot\mathbf{u}_\alpha^M e^{\frac{\gamma-\Gamma_\alpha}{2}t''}dt''dt'\,. \tag{S6}$$

The time-dependence of angle and frequency degrees of freedom is then given by,

$$\delta\boldsymbol{\theta}(t) = \boldsymbol{M}^{-1/2}\delta\bar{\boldsymbol{\theta}}(t) = \sum_\alpha c_\alpha(t)\boldsymbol{M}^{-1/2}\mathbf{u}_\alpha^M\,, \tag{S7}$$

$$\delta\dot{\boldsymbol{\theta}}(t) = \boldsymbol{M}^{-1/2}\delta\dot{\bar{\boldsymbol{\theta}}}(t) = \sum_\alpha \dot{c}_\alpha(t)\boldsymbol{M}^{-1/2}\mathbf{u}_\alpha^M\,. \tag{S8}$$

The variances $p_1(t)$ and $p_2(t)$ of the angle and frequency deviations read,

$$p_1(t) = \delta\boldsymbol{\theta}^2(t) = \sum_{\alpha,\beta} c_\alpha(t)c_\beta(t)\mathbf{u}_\beta^{M\top}\boldsymbol{M}^{-1}\mathbf{u}_\alpha^M\,, \tag{S9}$$

$$p_2(t) = \delta\dot{\boldsymbol{\theta}}^2(t) = \sum_{\alpha,\beta} \dot{c}_\alpha(t)\dot{c}_\beta(t)\mathbf{u}_\beta^{M\top}\boldsymbol{M}^{-1}\mathbf{u}_\alpha^M\,. \tag{S10}$$

When $d_i = d = \gamma m_i\ \forall i$, both matrices $\mathbb{L}$ and $\mathbb{L}^M$ have the same eigenvectors and $\lambda_\alpha^M = \lambda_\alpha/m$. We assume homogeneous inertia and damping factor for the calculations in the next two paragraphs.

**Correlated Noisy disturbances**

In the case of stochastic disturbances that persist in time, we average the $p_i$'s as follows,

$$\mathcal{P}_i = \lim_{T\to\infty} T^{-1}\int_0^T \overline{p_i(t)}dt\ \,,\ i=1,2\,, \tag{S11}$$

where $\overline{p_i(t)}$ indicates an average taken over the ensemble defined by e.g. the moments of the stochastic disturbance. We consider Ornstein-Uhlenbeck correlated noise on a single node, $k$, with zero mean $\overline{\delta P_k(t)} = 0$ and second moment $\overline{\delta P_i(t_1)\delta P_j(t_2)} = \delta_{ik}\delta_{jk}\,\delta P_0^2\exp[-|t_1-t_2|/\tau_0]$, correlated over a typical time scale $\tau_0$ and uniform inertia and damping. We have,

$$\mathcal{P}_1 = \lim_{T\to\infty} T^{-1}\sum_{\alpha\geq 2}\int_0^T \overline{c_\alpha^2(t)}dt \tag{S12}$$

$$= \lim_{T\to\infty} T^{-1}\sum_{\alpha\geq 2}\int_0^T e^{-(\gamma+\Gamma_\alpha)t}\int_0^t\int_0^t e^{\Gamma_\alpha(t_1'+t_2')}\times \tag{S13}$$

$$\int_0^{t_1'}\int_0^{t_2'}\sum_{i,j}\frac{u_{\alpha,i}u_{\alpha,j}}{m}\,\overline{\delta P_i(t_1'')\delta P_j(t_2'')}\,e^{\frac{\gamma-\Gamma_\alpha}{2}(t_1''+t_2'')}\,dtdt_1'dt_2'dt_1''dt_2''\,.$$

For homogeneous damping and inertia one has $\Gamma_\alpha = \sqrt{\gamma^2 - 4\lambda_\alpha/m}$. The integrals can be performed straightforwardly and one obtains

$$\mathcal{P}_1 = \delta P_0^2 \sum_{\alpha\geq 2} \frac{u_{\alpha,k}^2(\tau_0 + m/d)}{\lambda_\alpha(\lambda_\alpha\tau_0 + d + m\tau_0^{-1})} \,, \tag{S14a}$$

$$\mathcal{P}_2 = \delta P_0^2 \sum_{\alpha\geq 2} \frac{u_{\alpha,k}^2}{d(\lambda_\alpha\tau_0 + d + m\tau_0^{-1})} \,. \tag{S14b}$$

Taking the two limits $\lambda_\alpha\tau_0 \gg d$, $\lambda_\alpha\tau_0^2 \gg m$ and $\lambda_\alpha\tau_0 \ll d$, $\lambda_\alpha\tau_0^2 \ll m$, Eqs. (6a,b) of the main text are then easily obtained. Note that the above computation can be done relaxing the uniform inertia and damping hypothesis. The performance measures for Kuramoto oscillators are obtained for $m = 0$ [S1]. The asymptotics are then obtained by taking the asymptotic limits of large/small $\tau_0$ only after setting $m = 0$. One obtains,

$$\mathcal{P}_1 = \begin{cases} \big(\delta P_0^2\tau_0\big)/d\big)\left(C_1^{-1}(k) - n^{-2}Kf_1\right) \;\;, \; \lambda_\alpha\tau_0 \ll 1\,, \\ \delta P_0^2\left(C_2^{-1}(k) - n^{-2}Kf_2\right) \;\;, \; \lambda_\alpha\tau_0 \gg d\,, \end{cases} \tag{S15a}$$

$$\mathcal{P}_2 = \begin{cases} \big(\delta P_0^2\tau_0/d\big)\big(n-1\big)/n \;\;, \; \lambda_\alpha\tau_0 \ll 1\,, \\ \big(\delta P_0^2/d\tau_0\big)\left(C_1^{-1}(k) - n^{-2}Kf_1\right) \;\;, \; \lambda_\alpha\tau_0 \gg d\,, \end{cases} \tag{S15b}$$

where we use the generalized resistance centralities $C_{1,2}(i)$ and Kirchhoff indices $Kf_{1,2}$ discussed in Section  below.

**Box disturbances**

The same kind of computation as for the noisy disturbance can be done with a box disturbance acting on node $k$, i.e. $\delta P_i(t) = \delta_{ik}\,\delta P_0\,\Theta(t)\Theta(\tau_0 - t)$ with the Heaviside step function $\Theta(t) = 0$ for $t < 0$ and $\Theta(t) = 1$ for $t \geq 1$. As the perturbation is limited in time, we consider the performance measures,

$$\mathcal{P}_1^\infty = \sum_i \int_0^\infty |\delta\theta_i - \Delta(t)|^2 dt \,, \tag{S16}$$

$$\mathcal{P}_2^\infty = \sum_i \int_0^\infty |\delta\dot{\theta}_i - \dot{\Delta}(t)|^2 dt \,, \tag{S17}$$

instead of (S11). For uniform inertia and damping one obtains,

$$\mathcal{P}_1^\infty = \frac{\delta P_0^2 m}{8\gamma} \sum_{\alpha\geq 2} \frac{u_{\alpha,k}^2}{\Gamma_\alpha\lambda_\alpha^3}\left[2\Gamma_\alpha(4\gamma\tau_0\lambda_\alpha/m - 3\gamma^2 - \Gamma_\alpha^2) + (\gamma+\Gamma_\alpha)^3 e^{-\tau_0\frac{(\gamma-\Gamma_\alpha)}{2}} - (\gamma-\Gamma_\alpha)^3 e^{-\tau_0\frac{(\gamma+\Gamma_\alpha)}{2}}\right] ,$$

$$\mathcal{P}_2^\infty = \frac{\delta P_0^2}{2d} \sum_{\alpha\geq 2} \frac{u_{\alpha,k}^2}{\Gamma_\alpha\lambda_\alpha}\left[2\Gamma_\alpha - (\gamma+\Gamma_\alpha)e^{-\frac{\tau_0(\gamma-\Gamma_\alpha)}{2}} + (\gamma-\Gamma_\alpha)e^{-\frac{\tau_0(\gamma+\Gamma_\alpha)}{2}}\right] ,$$

with $\Gamma_\alpha = \sqrt{\gamma^2 - 4\lambda_\alpha/m}$. The two asymptotic limits of large and small $\tau_0$ are given by,

$$\mathcal{P}_1^\infty = \begin{cases} \left(\delta P_0^2 \tau_0^2/2d\right)\left(C_1^{-1}(k) - n^{-2}Kf_1\right) \ , \ (\gamma \pm \Gamma_\alpha)\tau_0 \ll 1 \, , \\ \delta P_0^2 \tau_0 \left(C_2^{-1}(k) - n^{-2}Kf_2\right) \ , \ (\gamma \pm \Gamma_\alpha)\tau_0 \gg 1 \text{ and } \lambda_\alpha \tau_0/d \gg 1 \, , \end{cases} \tag{S18a}$$

$$\mathcal{P}_2^\infty = \begin{cases} \left(\delta P_0^2 \tau_0^2/2md\right)\left(n-1\right)/n \ , \ (\gamma \pm \Gamma_\alpha)\tau_0 \ll 1 \, , \\ \left(\delta P_0^2/d\right)\left(C_1^{-1}(k) - n^{-2}Kf_1\right) \ , \ (\gamma \pm \Gamma_\alpha)\tau_0 \gg 1 \, , \end{cases} \tag{S18b}$$

which are also given by resistance centralities and Kirchhoff indices.

## RESISTANCE DISTANCES, CENTRALITIES AND KIRCHHOFF INDICES

The resistance centralities $C_1$ and $C_2$ can be expressed as functions of the distribution of resistance distances $\Omega_{ij}$, between any pairs of nodes $(i, j)$ of the network. The Laplacian matrix $\mathbb{L}$ of the network has one zero eigenvalue associated to the constant eigenvector $u_{1,i} = 1/\sqrt{n}$, its pseudoinverse $\mathbb{L}^\dagger$ is defined by [S2],

$$\mathbb{L}\mathbb{L}^\dagger = \mathbb{L}^\dagger\mathbb{L} = \mathbb{I} - \mathbf{u}_1^\top \mathbf{u}_1 \, , \tag{S19}$$

from which the resistance distance between nodes $i$ and $j$ is expressed as,

$$\Omega_{ij} = \mathbb{L}^\dagger_{ii} + \mathbb{L}^\dagger_{jj} - \mathbb{L}^\dagger_{ij} - \mathbb{L}^\dagger_{ji} \, . \tag{S20}$$

Using the eigenvectors of $\mathbb{L}$ we can rewrite Eq. (S20) as [S1],

$$\Omega_{ij} = \sum_{\alpha \geq 2} \frac{(u_{\alpha,i} - u_{\alpha,j})^2}{\lambda_\alpha} \, . \tag{S21}$$

The resistance distance is a graph metric in the sense that : i) $\Omega_{ii} = 0$, $\forall i$, ii) $\Omega_{ij} \geq 0$, $\forall i, j$, and iii) $\Omega_{ij} + \Omega_{jk} \geq \Omega_{ik}$, $\forall i, j, k$ (triangle inequality) [S2]. The Kirchhoff index of a network is obtained from the resistance distances by summing over all pairs of nodes, [S2]

$$Kf_1 = \sum_{i<j} \Omega_{ij} = n \sum_{\alpha \geq 2} \lambda_\alpha^{-1} \, . \tag{S22}$$

The Kirchhoff index is, up to a normalization factor, the mean resistance distance over the whole graph.

We generalize this definition of the resistance distance for matrices that are powers of the original Laplacian matrix, $\mathbb{L}' = \mathbb{L}^p$ and thus $[\mathbb{L}']^\dagger = \left[\mathbb{L}^p + \mathbf{u}_1^\top \mathbf{u}_1\right]^{-1}$. One has

$$\Omega_{ij}^{(p)} = [\mathbb{L}'_{ii}]^\dagger + [\mathbb{L}'_{jj}]^\dagger - [\mathbb{L}'_{ij}]^\dagger - [\mathbb{L}'_{ji}]^\dagger \, . \tag{S23}$$

The eigenvectors of $\mathbb{L}'$ are the same as those of $\mathbb{L}$. Thus we have,

$$\Omega_{ij}^{(p)} = \sum_{\alpha \geq 2} \frac{(u_{\alpha,i} - u_{\alpha,j})^2}{\lambda_\alpha^p} \ . \tag{S24}$$

We still have to check that the generalized resistance distances $\Omega_{ij}^{(p)}$ have the three properties of a graph metric. We remark that $\Omega_{ij}^{(p)}$ corresponds to the resistance distance between nodes $i$ and $j$ in a new graph whose Laplacian is $\mathbb{L}' = \mathbb{L}^p$. Therefore it is sufficient to show that $\mathbb{L}'$ is also a Laplacian matrix. to that end we demonstrate that the product of two Laplacian matrices $\mathcal{A}$ and $\mathcal{B}$ is still a Laplacian matrix. For a Laplacian matrix $\mathcal{A}$ one has (i) $\sum_i \mathcal{A}_{ij} = 0$, (ii) $\mathcal{A}_{ii} = -\sum_{j \neq i} \mathcal{A}_{ij}$. From these generic properties of Laplacian matrices, matrix elements of the product $\mathcal{AB}$ satisfy

$$\sum_j [\mathcal{AB}]_{ij} = \sum_{j,k} \mathcal{A}_{ik} \mathcal{B}_{kj} = 0 \ , \tag{S25}$$

$$\sum_{j \neq i} [\mathcal{AB}]_{ij} = \sum_j [\mathcal{AB}]_{ij} - [\mathcal{AB}]_{ii} = -[\mathcal{AB}]_{ii} \ . \tag{S26}$$

We conclude that the product $\mathcal{AB}$ is also a Laplacian matrix, and therefore, the generalized resistance distances $\Omega_{ij}^{(p)}$ have the three properties of a graph metric. With the generalized resistance distances, we can define generalized Kirchhoff indices [S1],

$$Kf_p = \sum_{i<j} \Omega_{ij}^{(p)} = n \sum_{\alpha \geq 2} \lambda_\alpha^{-p} \ . \tag{S27}$$

The relation between the resistive centrality $C_1(i)$ and the resistance distance is obtained from Eqs. (S21) and (S22),

$$C_1(i) = \left[ n^{-1} \sum_j \Omega_{ij} \right]^{-1} = \left[ \sum_{\alpha \geq 2} \frac{u_{\alpha,i}^2}{\lambda_\alpha} + n^{-2} Kf_1 \right]^{-1} \ . \tag{S28}$$

The expression for $C_2(i)$ involves higher moments of the distribution of resistance distances. We obtain

$$C_2(i) = \sum_j \Omega_{ij}^2 - n\, C_1^{-2}(i) + 2 \sum_j \Omega_{ij}\, C_1^{-1}(j) - 4\, C_1^{-1}(i)\, n^{-1} Kf_1 - 3 \sum_j C_1^{-2}(j) + 12 n^{-3} Kf_1^2 \ .$$

## NUMERICAL MODELS

We checked our analytical results against numerical ones obtained for four different models which we briefly describe here.

**European electric power grid**

We have constructed a model of the European high voltage electrical grid. It is composed of 3809 consumer and generator nodes connected to one another by 4944 lines. The geographic location of each node and the location of the lines between them has been extracted from the ENTSO-E database [S3]. Line capacities $b_{ij}$ between nodes have been normalized proportionally to the inverse of their length. The operational states (injections and consumptions) of the power grid are obtained via an optimal power flow which constrains the load flows on each line with the thermal limit of the latter and takes into account technical specificities for each power plant [S4, S8]. The two operational states considered in Figs. 3 and 4c of the main text correspond to a typical electric power consumption situation in winter (blue) and a case reproducing the extraordinary situation of November 2016, with a relatively high power demand and twenty french nuclear reactors offline (red). For the numerical simulations in Fig. 1 of the main text, we used the first case. For this model, the network Laplacian matrix has a spectrum distributed in the interval $\lambda_\alpha \in [0.0458, 26678.4395]$ (in the per unit system [S5]).

**IEEE 57 bus test case**

The IEEE 57 bus test case is a standardly used model of an electric power grid [S6]. It is composed of 57 buses including 7 generators and 80 lines. In Fig.4a of the main text, we use the tabulated operational state as well as a state where the tabulated loads are increased by a factor six [S6]. The spectrum of the Laplacian is distributed in the interval $\lambda_\alpha \in [0.2796, 118.6186]$ (in the per unit system [S5]).

Fig. S1 shows data similar to Fig. 1 in the main text for the IEEE 57 bus test case. The insets shows the asymptotic limits of very large and very small $\tau_0$, where $\mathcal{P}_{1,2}$ are predicted to be linear functions of the resistance centralities $C_{1,2}$ (see main text).

**MATPOWER Pegase 2869 Test Case**

The MATPOWER test case Pegase 2869 is a model representing a part of the European high voltage transmission grid [S4]. It is composed of 2869 buses including 510 generators and 4582 lines. In Fig.4b of the main text, we use the tabulated operational state as well as a state where injections are 30% larger [S4].The spectrum of the Laplacian is distributed in the interval $\lambda_\alpha \in [0.03536, 27156.901]$ (in the per unit system [S5]). Fig. S2 shows data similar to Fig. 1 in the main

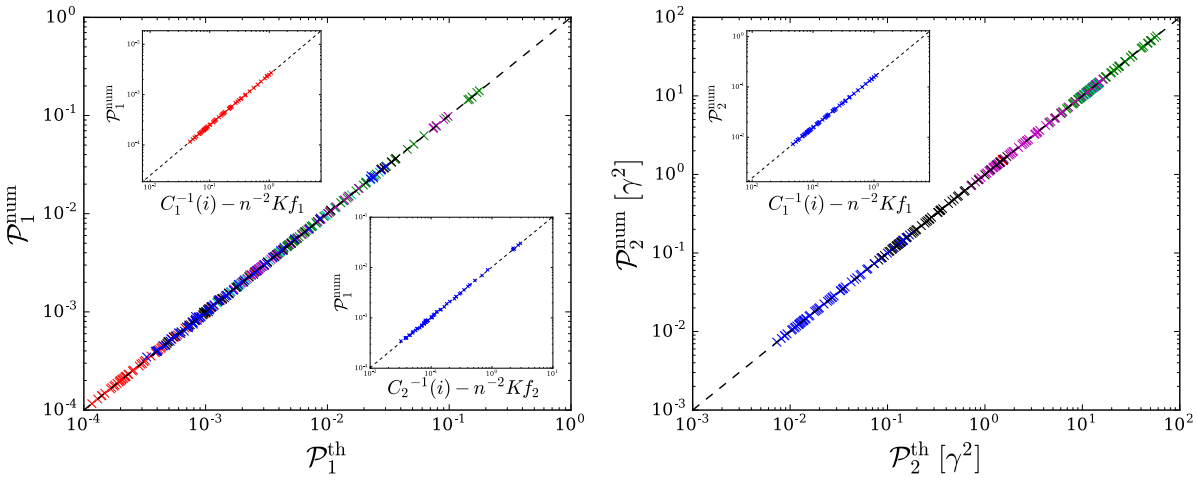



Figure S1. Comparison between theoretical predictions and numerical results for both performance measures $\mathcal{P}_1$ and $\mathcal{P}_2$. Each point corresponds to a noisy disturbance on a single node of the IEEE 57 bus test case [S6] with magnitude $\delta P_0 = 0.1$ and correlation times $\gamma\tau_0 = 4 \cdot 10^{-4}$ (red crosses), $4 \cdot 10^{-3}$ (cyan), $4 \cdot 10^{-2}$ (green), $4 \cdot 10^{-1}$ (purple), 4 (black) and 40 (blue). Time scales are defined by the ratio of damping to inertia coefficients $\gamma = d_i/m_i = 0.4s^{-1}$ which is assumed constant with $d_i = 0.004s$. The insets show $\mathcal{P}_1$ and $\mathcal{P}_2$ as a function of the resistance distance-based graph-theoretic predictions of Eqs. (5) in the main text, valid in both limits of very large and very short noise decorrelation time $\tau_0$. Not shown is the limit of short $\tau_0$ for $\mathcal{P}_2$, which gives a node-independent result.

text for this model.

**Random Network**

We finally used a random network obtained by random rewiring of edges with probability 0.5 of a single-cycle network with 1000 nodes with nearest and next-to-nearest couplings [S7]. Edges have the same weight $b_{ij} = b_0 = 1s^{-1}$. The spectrum of the Laplacian is distributed in the interval $\lambda_\alpha \in [0.39b_0, 10.47b_0]$.

In our numerics, we define a first-order, inertialess Kuramoto model on this random network. Fig.4d of the main text considers various distribution of natural frequencies, including one (green) which is close to instability with angle differences larger than $90^o$.

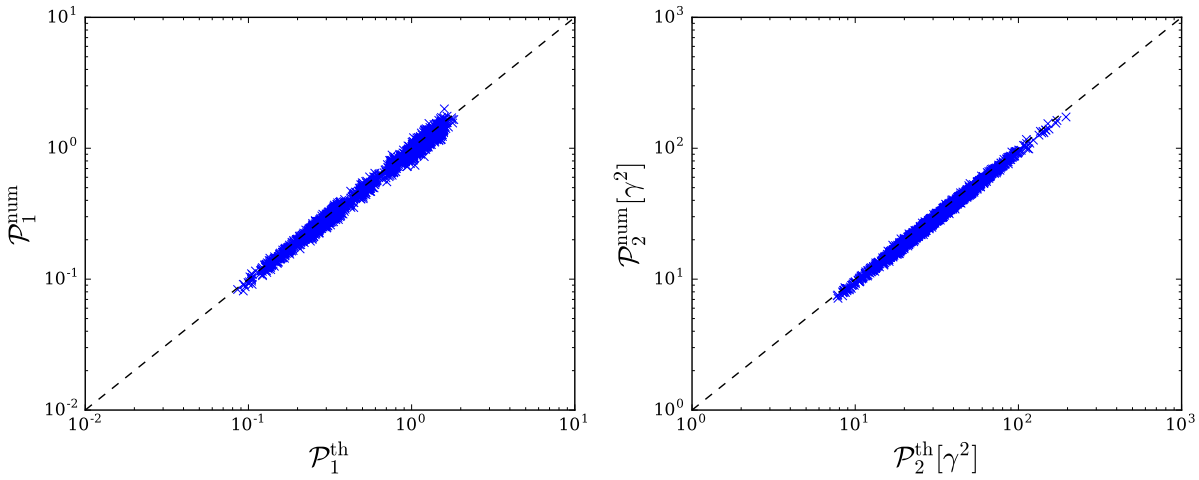



Figure S2. Comparison of the performance measures $\mathcal{P}_1$, $\mathcal{P}_2$ obtained numerically and Eqs. (S14). Each point corresponds to a noisy disturbance on a single node of the Pegase 2869 test case [S4] with magnitude $\delta P_0 = 0.1$ and correlation time $\gamma\tau_0 = 0.4$ and ratio of damping to inertia $\gamma = 0.4s^{-1}$ with $d_i = 0.007s$.

## NUMERICAL COMPARISON OF LRANK WITH WLRANK

In Fig.5 of the main text, we calculated the percentage of nodes with highest $\text{LRank}_2$ necessary to give the top 15 % ranked nodes with $\text{WLRank}_2$. The conclusions drawn from these data are generic – they are valid for different percentages than 15% and for $\text{LRank}_1$ vs. $\text{WLRank}_1$. This is illustrated in Fig. S3, which shows similar results for the percentage of nodes with highest $\text{LRank}_{1,2}$ that include the top 10% and 20% ranked nodes with $\text{WLRank}_{1,2}$.


[S1] M. Tyloo, T. Coletta and Ph. Jacquod, *Robustness of Synchrony in Complex Networks and Generalized Kirchhoff Indices*, Phys. Rev. Lett. **120**, 084101 (2018).

[S2] D.J. Klein and M. Randić, *Resistance Distances*, J. Math. Chem. **12**, 81 (1993).

[S3] B. Wiegmans, *GridKit Extract of ENTSO-E Interactive Map*, doi.org/10.5281/zenodo.55853 (2016).

[S4] R. D. Zimmerman, C. E. Murillo-Sánchez, and R. J. Thomas, *MATPOWER: Steady-State Operations, Planning and Analysis Tools for Power Systems Research and Education*, IEEE Trans. on Power Systems **26**, 12 (2011).

[S5] J. Machowski, J.W. Bialek, and J.R. Bumby, *Power System Dynamics: Stability and Control* 2nd Ed., John Wiley and Sons (2011).

[S6] University of Washington, Electrical Engineering, *Power systems test case archive*, www2.ee.washington.edu/research/pstca, (1993).

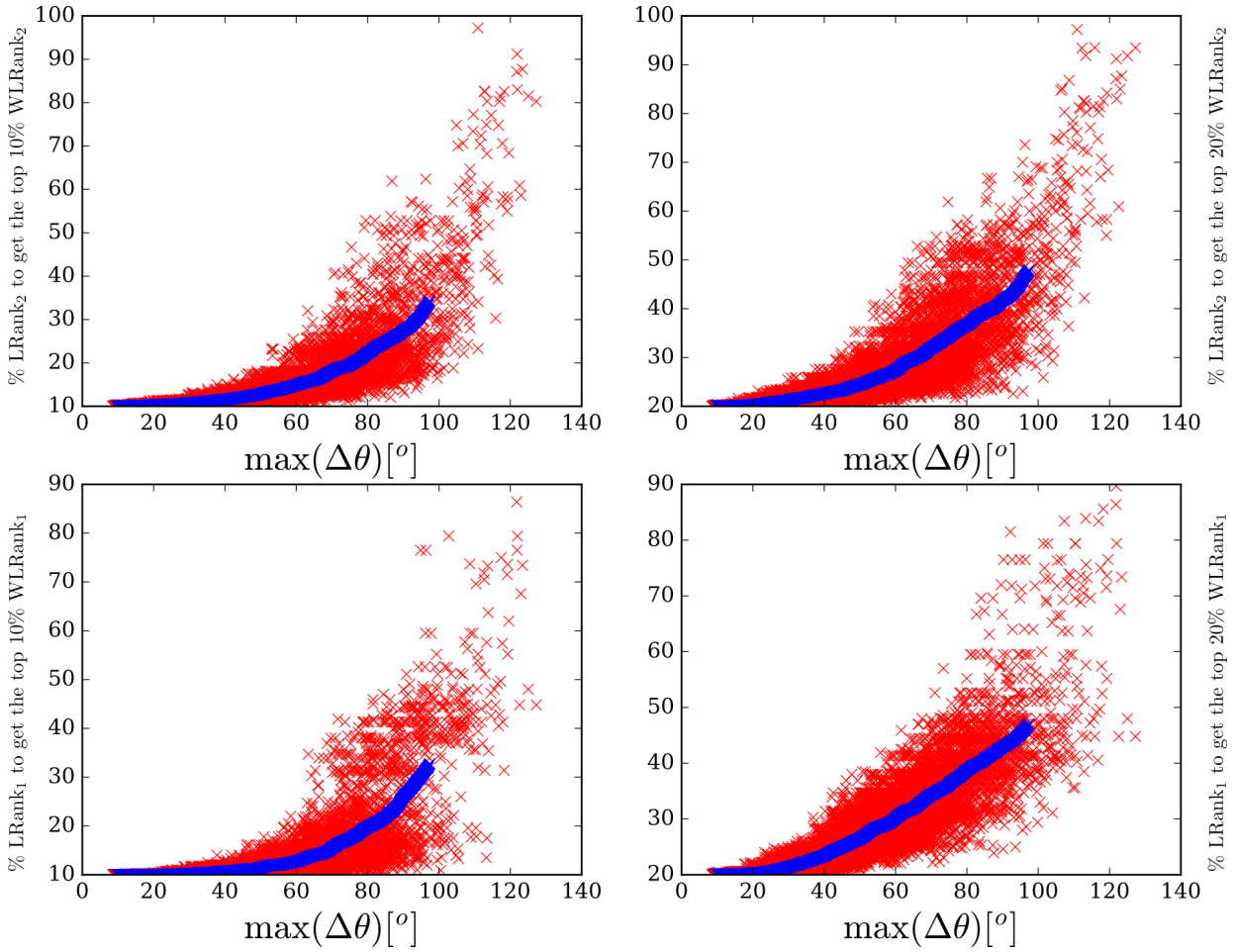



Figure S3. Percentage of the nodes with highest $\mathrm{LRank}_{1,2}$ necessary to give the top 10 % (left), 20% (right) ranked nodes with $\mathrm{WLRank}_{1,2}$ for a random network of inertialess coupled oscillators with 1000 nodes obtained by rewiring with probability 0.5 a cyclic graph with constant nearest and next-to-nearest neighbor coupling (supplementary materials, materials and methods). Each of the 12000 red crosses corresponds to one of 1000 random natural frequency vector $\boldsymbol{P}^{(0)}$ with components randomly distributed in $[-0.5, 0.5]$ and summing to zero, multiplied by a prefactor $\beta = 0.4, 0.6, \ldots 2.6$. The blue crosses correspond to running averages over 500 red crosses with consecutive values of $\max(\Delta\theta)$.


[S7] D.J. Watts and S.H. Strogatz, *Collective Dynamics of 'Small World' Networks*, Nature **393**, 440 (1998).

[S8] L. Pagnier and Ph. Jacquod, *Disturbance propagation, inertia location and slow modes in large-scale high voltage power grids*, arXiv:1810.04982 (2018).